*Materials Sciences and Applications*, 2010, 1, 217-222
doi:10.4236/msa.2010.14034 Published Online October 2010 (http://www.SciRP.org/journal/msa)

# Nanoindentation Study of Al356-$Al_2O_3$ Nanocomposite Prepared by Ball Milling

**Yousef Mazaheri, Fathallah Karimzadeh*, Mohammad-Hosein Enayati**

Department of Materials Engineering, Nanotechnology and Advanced Materials Institute (NAMI), Isfahan University of Technology, Isfahan, Iran.
Email: karimzadeh_f@cc.iut.ac.ir

Received May 4th, 2010; revised May 31st, 2010; accepted June 6th, 2010.

## ABSTRACT

*In this study ball milling of Al*356 *and* $Al_2O_3$ *powder mixture was carried out in order to produce Al*356-$Al_2O_3$ *nanocomposite containing* 20 *vol.%* $Al_2O_3$*. The structural evolution and morphological changes of powder particles during ball milling were studied by X-ray diffractometery and scanning electron microscopy analysis. As a result of ball milling* $Al_2O_3$ *particles were uniformly dispersed in Al*356 *matrix. Furthermore the crystallite size of the Al*356 *decreased to* 25 *nm after ball milling for* 10 *h. Morphological studies of powder particles indicated that the powder particle size continuously decreases with increasing milling time. Hardness and elastic modulus values of powder particles were measured by nanoindentation method. It was found that the hardness and elastic modulus of Al*356-20 *vol.%* $Al_2O_3$ *nanocomposite were about* 216 *Hv and* 86 *GPa, respectively which is higher than* 75 *Hv and* 74 *GPa for as-received Al*356*.*

***Keywords***: *Al-*$Al_2O_3$ *Nanocomposite*, *Nanocrystalline Structure*, *Ball Milling*, *Nanoindentation*

## 1. Introduction

Metal matrix composites (MMCs) are under attention for many applications in aerospace, defense, and automobile industries. These materials have been considered for using in automobile brake rotors and various components in internal combustion engines because of its high strength/weight ratio and wear resistance [1]. Al is the most popular matrix for MMCs because of its low density, good corrosion resistance and high thermal and electrical conductivity [2,3]. Conventional Al matrix composites (AMCs) reinforced with ceramic particulates, especially $Al_2O_3$ exhibit high strength, hardness and elastic modulus [4].

AMCs have been widely studied since the 1920s [2]. A survey of the previous studies indicates that a homogenous dispersion of fine particles in a fine grained matrix is beneficial to the mechanical properties of MMCs [5-10]. The use of Al-$Al_2O_3$ has been limited due to high processing cost [11]. Solid state processes such as ball milling (BM) can be readily used to fabricate Al-$Al_2O_3$ composite with improved properties [12]. For instance; Tavoosi *et al.* [13] used high energy BM to prepare Al-$Al_2O_3$ nanocomposite and showed that the hardness and wear resistance increased with increasing $Al_2O_3$ content of the nanocomposites. BM is well recognized as a potential method for achieving better dispersion of reinforcing particles in the matrixes of micro- and nanocomposites. The BM process involves repeated plastic deformation, welding and fracture of powder particles [4]. Addition of ceramic reinforcements into a ductile matrix has a great effect on the structural evolution during BM. Although there have been several research studies about the effect of milling parameters, such as ball sizes, number of balls and milling time on the microstructure of Al-$Al_2O_3$ composites , for example [1,14-18], the effect of nanocrystalline structure reinforced with ceramic particulates on properties of Al-$Al_2O_3$ nanocomposites is not well investigated yet. The objective of the present work is to investigate the properties of micrometric $Al_2O_3$ reinforced Al356 matrix composite prepared by BM technique. The addition of $Al_2O_3$ particles to residual machining chips of Al356 display an effective cost saving in this work.

## 2. Materials and Methods

### 2.1. Samples Preparation

Residual machining chips of A356 aluminum alloy (Al356) and α-$Al_2O_3$ powder with purity of 99% were used as starting materials. **Table 1** lists chemical analysis of the Al356 chips. **Figure 1** shows scanning electron micros-

 

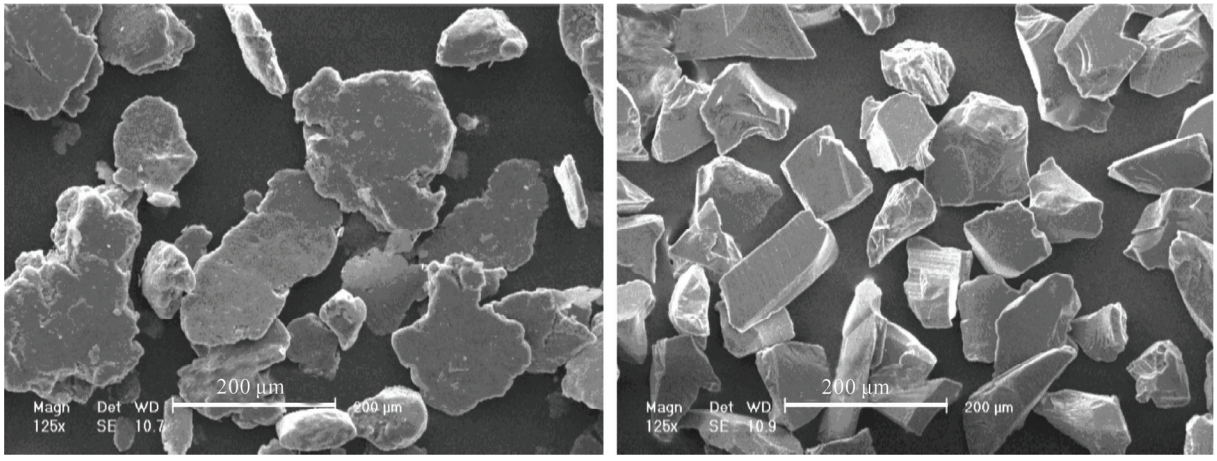


(a) (b)

**Figure 1. SEM images of as-received materials. (a) Al356 chips; (b) $Al_2O_3$ powder particles.**

**Table 1. Chemical composition of Al356 chips.**

| Element | Al | Si | Mg | Fe | Mn | Cu | Ti |
|---|---|---|---|---|---|---|---|
| Composition (wt. %) | Rem | 7.44 | 0.44 | 0.26 | 0.07 | 0.05 | 0.02 |

copy micrographs of as-received materials. Al356 chips were irregular in shape with a size distribution of 200-300 µm and $Al_2O_3$ powder particles had an angular shape with a size distribution of 100-200 µm.

The Al356 chips and $Al_2O_3$ powder particles were mixed to achieve Al356-20 vol. % $Al_2O_3$ composition. BM was carried out in a high energy planetary ball mill (PM 100), nominally at room temperature and under Ar atmosphere. The milling media consisted of twenty 20 mm diameter balls confined in a 500 ml volume vial. The ball and vial materials were hardened chromium steel. Ball to powder weight ratio and rotation speed of vial was 6:1 and 300 rpm, respectively. The total powder mass was 100 gr and 0.3 wt. % stearic acid was added as a process control agent (PCA).

## 2.2. Analysis Techniques

Samples were taken at selected time intervals and characterized by X-ray diffraction (XRD) in a Philips XPERT MPD diffractometer using filtered Cu $K_\alpha$ radiation ($\lambda$ = 0.1542 nm). Morphology and microstructure of powder particles were characterized by scanning electron microscopy (SEM) in a Philips XL30.

The crystallite size and lattice strain of powders were estimated using the Williamson-Hall method by following equation [19]:

$$\beta \cos\theta = \frac{K\lambda}{D} + 2A\sqrt{(\varepsilon)^2}\sin\theta \qquad (1)$$

where $\theta$ is the Bragg diffraction angle, $D$ the crystallite size, $\varepsilon$ the average internal strain, $\lambda$ the wave length of the radiation used, $\beta$ the diffraction peak width at half maximum intensity, $K$ the Scherrer constant (0.9) and $A$ is the coefficient which depends on the distribution of strain; it is near to unity for dislocations.

## 2.3. Nanoindentation Method

Depth sensing indentation (DSI) is commonly referred to as nanoindentation since the technique usually operates in the submicron depth range with nanometer resolution [20-24]. DSI differs from classical hardness measurements (Vickers, Brinell and Knoop), where the impressions are first generated, and then imaged using a microscopy technique. The nanoindentation test involves indenting a specimen with a very low load using a high precision instrument, which records the load and penetration depth continuously. The mechanical properties can be derived from the measured load-penetration depth curves under loading/unloading through appropriate data analysis. **Figure 2** shows a typical load-penetration depth curve obtained in a nanoindentation test. The peak indentation depth is denoted by $h_m$ and includes elastic and plastic deformation. The depth at which the applied loads become zero on unloading is the final indentation depth $h_f$ and represents the plastic deformation. $S$ represents the contact stiffness measured during the first moments of the unload operation. $S = dF/dh$ is the slope of the tangent of the load-penetration depth curve during the unloading cycle. The depth $h_c$ is the contact depth at which the cross-section area $A_p$ is taken to calculate hardness [25].

The contact depth $h_c$ and the hardness are calculated by a standard procedure according to the method of Oliver and Pharr [26]; $h_c$ can be written as:

$$h_c = h_m - \varepsilon\frac{F_m}{s} \qquad (2)$$

 

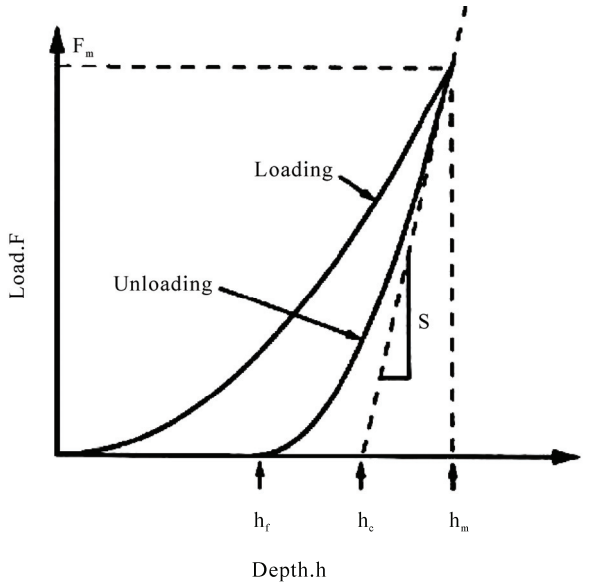


**Figure 2. Load versus penetration depth curve obtained from a nanoindentation test.**

Knowing $h_c$, $A_p$ is calculated. The instrumented hardness $H_{IT}$ is determined from peak load $F_m$ and projected area $A_p$ of contact as:

$$H_{IT} = \frac{F_m}{A_p} \tag{3}$$

Whereas the Vickers hardness $HV$ is calculated from the developed area $A_d$:

$$HV = \frac{F_m}{A_d} \tag{4}$$

The difference between an instrumented hardness and Vickers hardness resides in definition of the contact area between the indenter and the tested material.

A reduced modulus, $E_{IT}^*$, is used to account for the fact that the elastic displacements occur in both the indenter and the sample. This reduced elastic modulus can be linked to the measured stiffness $S$ by the relation:

$$E_{IT}^* = \frac{\sqrt{\pi}}{2}\frac{S}{\sqrt{A_p}} \tag{5}$$

Knowing $S$ and $A_p$, $E_{IT}^*$ is calculated.

The instrumented elastic modulus in the test material, $E_{IT}$, is determined by the relation:

$$E_{IT} = \frac{\left(1-\nu^2\right)}{\frac{1}{E_{IT}^*} - \frac{\left(1-\nu_i^2\right)}{E_i}} \tag{6}$$

where $\nu$ is the Poisson's ratio for the sample, $E_i$ and $\nu_i$ are the elastic modulus and Poisson's ratio, respectively, of the indenter.

The hardness and elastic modulus of Al356 and Al356-$Al_2O_3$ composite was evaluated from the load-penetration depth curves obtained in nanoindentation tests using a nanoindentation tester (NHTX S/N: 01-03119, CSM Instruments) with a Berkovich diamond indenter (B-J87). The elastic constants $E_i$ = 1141 GPa and $\nu_i$ = 0.07 are often used for a diamond indenter [27]. The indentation was made to a maximum load of about 70 mN and under loading and unloading rate of 140 mN/min. In order to take the repeatability into account, the test results were acquired from the average of four indentations.

## 3. Results and Discussion

### 3.1. Structural Evolution

**Figure 3** shows XRD patterns of Al356 and $Al_2O_3$ powder mixture at different milling times. As can be seen with increasing milling times the intensity of Al356 and $Al_2O_3$ diffraction peaks decreases and their width increases progressively as a result of refinement of crystallite size and enhancement of lattice strain. With increasing milling time the brittle particles ($Al_2O_3$) are uniformly dispersed in the ductile matrix (Al356) [28].

The variation of Al356 crystallite size and lattice strain as a function of milling time is shown in **Figure 4**. As can be seen in **Figure 4(a)**, with increasing milling time Al crystallite size gradually redused reaching a value of 25 nm after 10 h of milling time. Moreover, the lattice strain induced by milling increased up to 0.43% (**Figure 4(b)**). The crystallite size of the $Al_2O_3$ particles was calculated to be about 60 nm after 10h of milling time.

SEM images of powder particles at different milling times are shown in **Figure 5**. As seen after 2 h of milling time the powder particles had a flake morphology. with increasing milling time the powder particles size decreased to 10-20 μm due to the predominance of the fracturing of powder particles over the cold welding process. Also flake morphology changed to equeiaxed morphology with

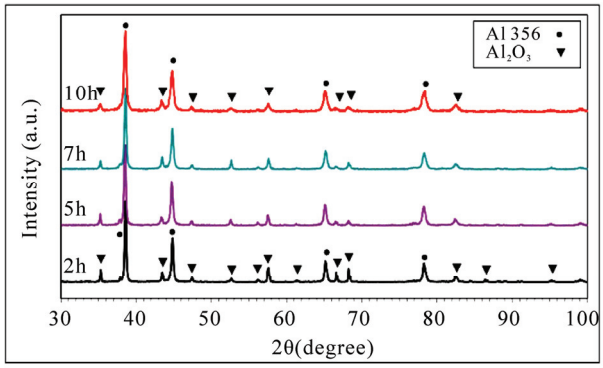


**Figure 3. XRD patterns of Al356 and $Al_2O_3$ powder mixture at different milling times.**

 

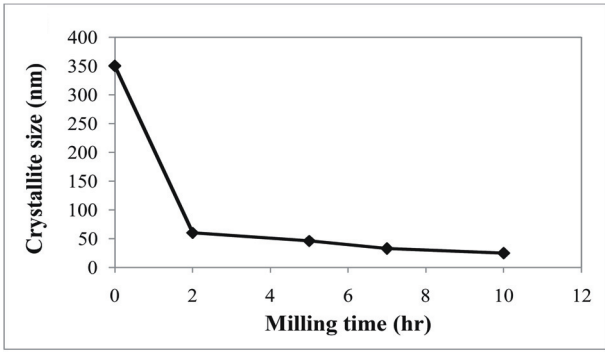


(a)

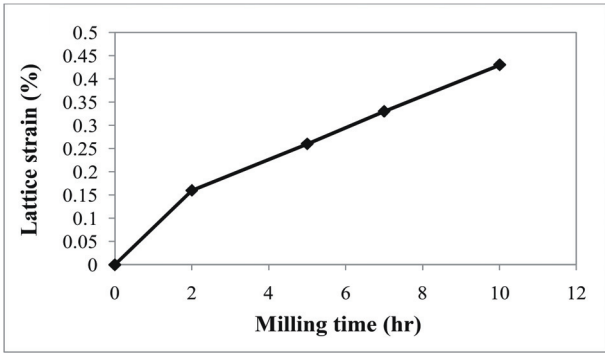


(b)

**Figure 4. The variation of (a) Al356 crystallite size; (b) lattice strain as a function of milling time.**

increasing milling time. At longer milling times the powder particles were more uniform in size compared to the early stages of milling. The larger particles at longer milling times appeared to be an agglomaration of many smaller particles.

### 3.2. Nanoindentation Profile

**Figure 6** shows the load-penetration depth curves obtained from nanoindentation test of as-received Al356 and Al356-20 vol.% $Al_2O_3$ nanocomposite after 10 h of milling times. The difference in hardness of the materials is apparent from the large difference in the peak depth. The data obtained from the analysis of load/unload curve, are given in **Table 2**. Hardness and elastic modulus values of Al356-$Al_2O_3$ nanocomposite showed considerable increase compared with Al356.

The possible strengthening mechanisms which may operate in particle-reinforced MMCs [29]:

1) Orowan strengthening.

2) Grain and substructure strengthening.

3) Quench hardening resulting from the dislocations generated to accommodate the differential thermal contraction between the reinforcing particles and the matrix.

4) Work hardening, due to the strain misfit between the elastic reinforcing particles and the plastic matrix.

**Table 2. The results obtained from nanoindentation tests.**

| Parameter | Value | | Dimension |
|---|---|---|---|
| | Al356 | Nanocomposite | |
| $F_m$ | 70.28 | 70.23 | mN |
| $h_m$ | 2066 | 1279 | nm |
| $h_f$ | 1625 | 702 | nm |
| $S$ | 0.2068 | 0.2353 | mN/nm |
| $h_c$ | 1811 | 1062 | nm |
| $Ap$ | $8.7 \times 10^7$ | $3 \times 10^7$ | nm² |
| $H_{IT}$ | 807 | 2334 | MPa |
| $HV$ | 75 | 216 | Vickers |
| $E_{IT}$ | 74 | 86 | GPa |
| $Epsilon$ | 0.75 | 0.73 | |

According to the characteristics of the microstructure, the better mechanical properties of Al356-$Al_2O_3$ nanocomposite can be attributed to 1) the nano grain size of the Al matrix following the classical Hall-Petch relationship, and 2) the Orowan strengthening due to the fine dispersion of $Al_2O_3$ particles. Rule of mixtures can be applied to calculate the hardness and elastic modulus of Al356-$Al_2O_3$ nanocomposite [30]:

$$H_c = H_m F_m + H_r F_r \quad (7)$$

$$E_c = E_m F_m + E_r F_r \quad (8)$$

$H_c$, $H_m$, and $H_r$, show the hardness of the composite, matrix and reinforcement, respectively. $E_c$, $E_m$, and $E_r$, show the elastic modulus of the composite, matrix and reinforcement, respectively. $F_m$ and $F_r$ are fractional volumes of matrix and reinforcement. Nanoindentation results show that the addition of 20vol. % $Al_2O_3$ in Al356 matrix increased the hardness and elastic modulus from 75 Hv and 74 GPa to 216 Hv and 86 GPa, respectively. Nanoindentation tests showed that hardness and elastic modulus of $Al_2O_3$ were about 880 Hv and 150 GPa, respectively [31]. Taking the data in **Table 2** for $H_{Al356}$ (75 Hv), $E_{Al356}$ (74 GPa) and $F_{Al356}$ (0.8), $F_{Al2O3}$ (0.2), equation 7 and 8 give $H_c$ = 236 Hv and $E_c$ = 89.2 GPa, which are in good agreement with the experimental values of 216 Hv and 86 GPa, respectively.

## 4. Conclusions

Ex-situ Al356-$Al_2O_3$ nanocomposite was produced by ball milling process. Structural evolution indicated that as a result of ball milling the $Al_2O_3$ particles are uniformly dispersed in ductile Al356 matrix. Crystallite size

 

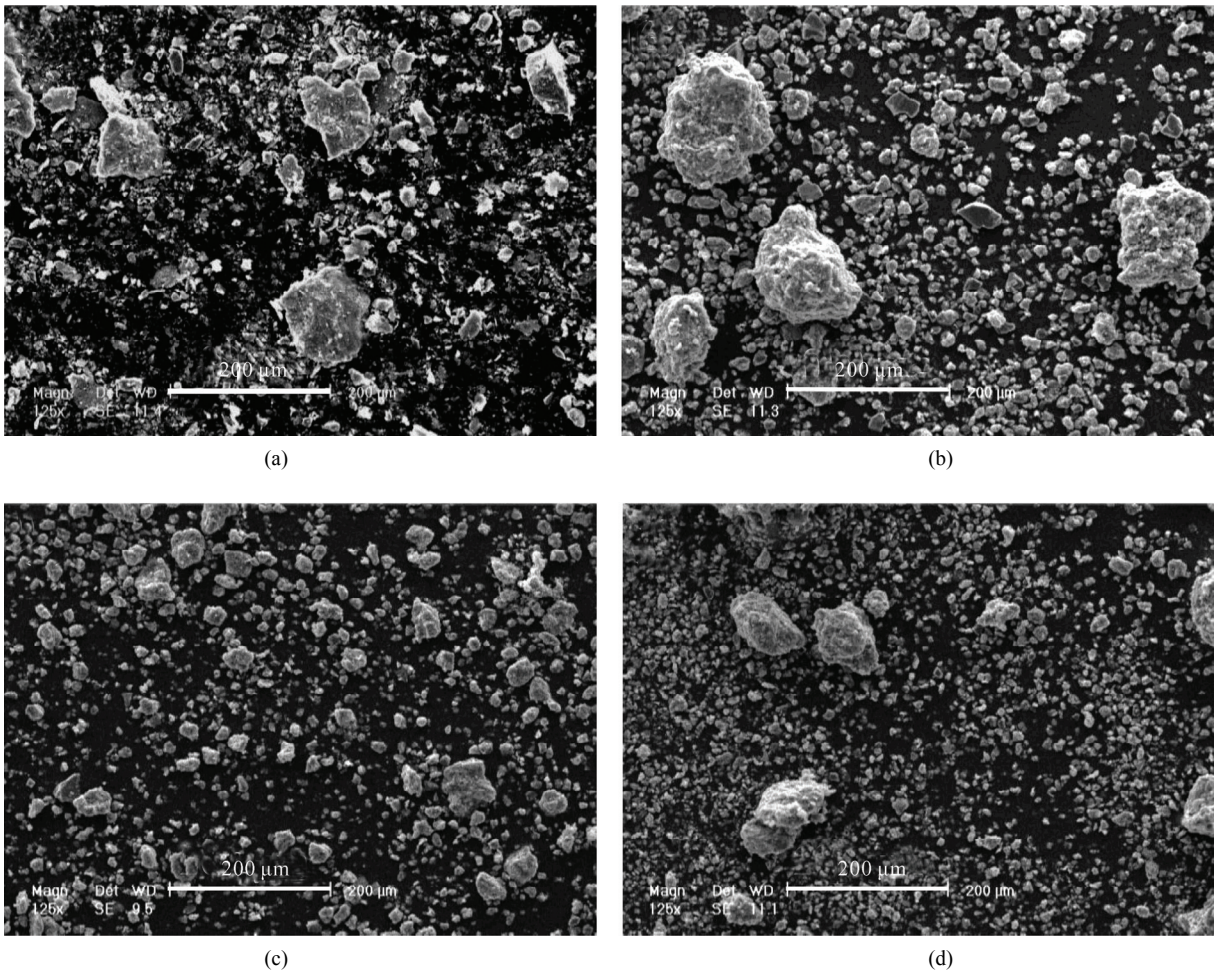


**Figure 5. SEM images of powder particles after (a) 2 h, (b) 5 h, (c) 7 h and (d) 10 h of milling times.**

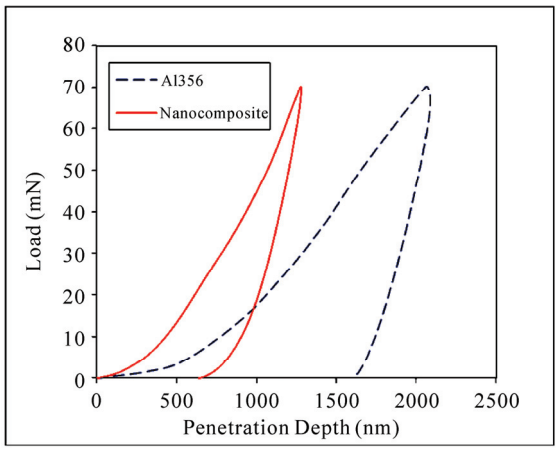


**Figure 6. Load versus penetration depth curves of Al356 and Al356-20 vol.% $Al_2O_3$ nanocomposite as-milled for 10 h.**

of Al matrix was 25 nm after 10 h of milling time. This microstructure led to a remarkable improvement of mechanical characteristics so that, for instance, the hardness and elastic modulus of Al356-20vol.% $Al_2O_3$ powder increased to 216 Hv and 86GPa, respectively.

## REFERENCES

[1] S. M. Zebarjad and S. A. Sajjadi, "Dependency of Physical and Mechanical Properties of Mechanical Alloyed Al-$Al_2O_3$ Composite on Milling Time," *Materials & Design*, Vol. 28, No. 7, 2007, pp. 2113-2120.

[2] V. Sethi, "Effect of Aging on Abrasive Wear Resistance of Silicon Carbide Particulate Reinforced Aluminum Matrix Composite," MSc. Thesis, University of Cincinnati, Cincinnati, 2007.

[3] A. Pyzalla, B. Camin, B. Lehrer, M. Wichert, A. Koch, K. Zimnik, E. Boller and W. Reimers, "In-Situ Observation of Creep Damage in Al-$Al_2O_3$ MMCs by Synchrotron X-Ray Tomography," International Centre for Diffraction Data, 2006, pp. 1097-2102.

[4] S. C. Tjong, "Novel Nanoparticle-Reinforced Metal Matrix Composites with Enhanced Mechanical Properties," *Advanced Engineering Materials*, Vol. 9, No. 8, 2007, pp. 639-652.

 

[5] I. A. Ibrahim, F. A. Mohamed and E. J. Lavernia, "Particulate Reinforced Metal Matrix Composite," *Journal of Matierals Science*, Vol. 26, 1991, pp. 1137-1156.

[6] A. Bhaduri, V. Gopinathan and P. Ramakrishnan, "Microstructural Changes in a Mechanically Alloyed Al-6.2 Zn-2.5 Mg-1.7 Cu Alloy (7010) with and without Particulate SiC Reinforcement," *Materials Transactions A*, Vol. 27, No. 11, 1995, pp. 3718-3726.

[7] A. Olszowka-Myalska, S. Janusz and J. Cwajna, "Characterization of Reinforcement Distribution in Al/$Al_2O_3$ System Composite Obtained from Composite Powder," *Character Material*, Vol. 46, No. 2-3, 2001, pp. 189-195.

[8] K. M. Shorowordi, T. Laoui, A. S. M. A. Haseeb and J. P. Celis, "Microstructure and Interface Characteristics of $B_4C$, SiC and $Al_2O_3$ Reinforced Al Matrix Composite: A Comparative Study," *Journal of Materials Processing Technology*, Vol. 142, No. 3, 2003, pp. 738-743.

[9] C. Shuangje and W. Renjie, "The Structure and Bending Properties of Squeeze-Cast Composites of A356 Aluminum Alloy Reinforced with Alumina Particles," *Composites Science and Technology*, Vol. 59, No. 1, 1999, pp. 157-162.

[10] B. Prabhu, C. Suryanarayana, L. An and R. Vaidyanathan, "Synthesis and Characterization of High Volume Fraction Al-$Al_2O_3$ Nanocomposite Powders by High-Energy Milling," *Materials Science and Engineering*, Vol. 425, No. 1-2, 2006, pp. 192-200.

[11] G. J. Howell and A. Ball, "Dry Sliding Wear of Particulate-Reinforced Aluminum Alloys against Automobile Friction Materials," *Wear*, Vol. 181-183, 1995, pp. 379-390.

[12] P. R. Soni, "Mechanical Alloying: Fundamentals and Applications," Cambridge International Science Publishing, Cambridge, 1999.

[13] M. Tavoosi, F. Karimzadeh and M. H. Enayati, "Wear Behaviour of Al-$Al_2O_3$ Nanocomposites Prepared by Mechanical Alloying and Hot Pressing," *Materials Science and Technology*, in Press.

[14] M. M. Moshksar and S. M. Zebarjad, "Effect of Milling Parameters on Milling of Metallic Powders," *Proceeding of Nonferrous Metals*, Kerman, 1996, pp. 913-917.

[15] M. M. Moshksar and S. M. Zebarjad, "Morphology and size Distribution of Aluminum Powder during Milling Processing," *Iranian Journal of Science and Technology*, Vol. 23, 1996, pp. 150-154.

[16] S. M. Zebarjad and S. A. Sajjadi, "Microstructure Evaluation of Al–$Al_2O_3$ Composite Produced by Mechanical Alloying Method," *Materials & Design*, Vol. 27, No. 8, 2006, pp. 684-688.

[17] Z. Razavi Hesabi, A. Simchi and S. M. Seyed Reihani, "Structural Evolution during Mechanical Milling of Nanometric and Micrometric $Al_2O_3$ Reinforced Al Matrix Composite," *Materials Science and Engineering A*, Vol. 428, No. 1-2, 2006, pp. 159-168.

[18] E. M. Ruiz-Navas, J. B. Fogagnolo, F. Velasco and L. Froyn, "One Step Production of Aluminum Matrix Composite Powder by Mechanical Alloying," *Composites Part A*, Vol. 37, No. 11, 2006, pp. 2114-2120.

[19] G. K. Williamson and W. H. Hall, "X-Ray Line Broadening from Filed Aluminium and Wolfram," *Acta Metallurgica*, Vol. 1, No. 1, 1953, pp. 22-31.

[20] W. C. Oliver and G. M. Pharr, "Measurement of Hardness and Elastic Modulus by Instrumented Indentation: Advances in Understanding and Refinements to Methodology," *Journal of Materials Research*, Vol. 19, No. 12, 2004, pp. 3-20.

[21] A. C. Fischer-Cripps, "Review of Analysis and Interpretation of Nanoindentation Test Data," *Surface and Coatings Technology*, Vol. 200, No. 14-15, 2006, pp. 4153-4165.

[22] C. A. Schuh, "Nanoindentation Studies of Materials," *Materials Today*, Vol. 9, 2006, pp. 32-49.

[23] A. Gouldstone, N. Chollacoop, M. Dao, J. Li, A. M. Minor and Y. L. Shen, "Indentation across Size Scales and Disciplines: Recent Developments in Experimentation and Modeling," *Acta Materialia*, Vol. 55, No. 12, 2007, pp. 4015-4039.

[24] Y. Golovin, "Nanoindentation and Mechanical Properties of Solids in Submicrovolumes, Thin Near-Surface Layers, and Films: A Review," *Physics of the Solid State*, Vol. 50, No. 12, 2008, pp. 2205-2236.

[25] C. L. Chen, A. Richter and R. C. Thomson, "Mechanical Properties of Intermetallic Phases in Multi-Component Al-Si Alloys Using Nanoindentation," *Intermetallics*, Vol. 17, No. 8, 2009, pp. 634-641.

[26] W. C. Oliver and G. M. Pharr, "An Improved Technique for Determining Hardness and Elastic-Modulus Using Load and Displacement Sensing Indentation Experiments," *Journal of Materials Research*, Vol. 7, No. 6, 1992, pp. 1564-1583.

[27] G. Simmons and H. Wang, "Single Crystal Elastic Constants and Calculated Aggregate Properties - A Handbook," MIT Press, Cambridge, 1971.

[28] C. Suryanarayana, "Mechanical Alloying and Milling," *Progress in Materials Science*, Vol. 46, No. 1-2, 2001, pp. 1-184.

[29] D. J. Lloyd, "Particle Reinforced Aluminium and Magnesium Matrix Composites," *International Materials Reviews*, Vol. 39, No. 1, 1994, pp. 1-24.

[30] G. E. Dieter, "Mechanical Metallurgy," 3rd Edition, McGraw-Hill, Berlin, 1976.

[31] T. C. Chou, T. G. Nieh, S. D. McAdams, G. M. Pharr and W. C. Oliver, "Mechanical Properties and Microstructures of Metal/Ceramic Microlaminates: Part II. A Mo/$Al_2O_3$ System," *Journal of Materials Research*, Vol. 7, No. 10, 1992, pp. 2774-2784.

 